

Materials Highlights

ISSN (Online): 2666-4933

ISSN (Print): N/A

Journal Home: <https://www.athena-publishing.com/journals/mahig>



Article Title

Structural and Optical Properties of BaO Nanoparticles Synthesized by Facile Co-Precipitation Method

Authors

Manauwar Ali Ansari, Nusrat Jahan

Corresponding Author

Manauwar Ali Ansari – maansarivce@gmail.com

Cite This Article As

M.A. Ansari, N. Jahan. Structural and Optical Properties of BaO Nanoparticles Synthesized by Facile Co-Precipitation Method. Materials Highlights, Vol. 2(1-2), pp. 23–28, 2021.

Link to This Article (DOI)

<https://doi.org/10.2991/mathi.k.210226.001>

Published on Athena Publishing Platform

31 January 2022

Research Article

Structural and Optical Properties of BaO Nanoparticles Synthesized by Facile Co-precipitation Method

Manauwar Ali Ansari^{1,*}, Nusrat Jahan²

¹Department of Material Science and Engineering, University of Miskolc, Miskolc, Egyetemvaros 3515, Hungary

²School of Science, JS University, Shikohabad, India

ARTICLE INFO

Article History

Received 07 November 2020

Accepted 24 February 2021

Keywords

Structural property
optical property
barium oxide
co-precipitation

ABSTRACT

This paper presents the synthesis of Barium Oxide Nanoparticles (BaO-NPs) on a large-scale by a simple and cost-effective co-precipitation method. The as-synthesized BaO-NPs were characterized in aspects of their structural, morphological, compositional, and optical properties. X-ray diffraction was done to assess the crystalline property of the nanomaterial and the crystallite size of the BaO-NPs was found to be 15–16 nm. Scanning electron microscopy was used to study the morphology of as-synthesized nanoparticles which confirmed that the prepared materials are flower-shaped nanoparticles. The compositional characteristics of nanoparticles were given by Fourier transform infrared spectroscopy which confirmed that the as-synthesized nanoparticles are pure BaO. A useful optical properties of nanoparticles were also reported via the room temperature UV-Vis and photoluminescence spectroscopy and calculated bandgap of the nanoparticles was found 4.65 eV.

© 2021 The Authors. Published by Atlantis Press B.V.

This is an open access article distributed under the CC BY-NC 4.0 license (<http://creativecommons.org/licenses/by-nc/4.0/>).

1. INTRODUCTION

Nanoscience and nanotechnology reveal a significant place in basic to applied material research because of their large number of applications which based on its size and design [1].

Transition metal oxide nanomaterials for example as copper oxide, iron oxide, Barium Oxide (BaO), tin oxide, zinc oxide, titanium oxide, etc. are known as being among the wealthiest nanomaterials family due to its increasing study and flexible applications [1–9], which have size-dependent materials properties compared to their bulk phases, making them widely used in various fields such as sensors, actuators, high-temperature superconductors, capacitors, environmental sciences, biomedical sciences, Li-ion batteries, solar cells, etc. An extensive study has been carried out in this field and published in the literature because of the wide range of applications of this type of material.

Among all the several other metal oxide nanomaterials, BaO is a direct band gap type, group II–VI semiconductor nanomaterial having unique significance due to their wide bandgap (4.4 eV [10]) and hygroscopic characteristics and large applications such as self-cleaning [11], electrical-energy generation [11], sensors and actuators [12–14], Pharmaceutical industry [15], catalysts [1,16]. Apart from this, BaO was seen significantly useful in electron field emission [10], conservation and restoration of cultural heritage such as paper-based artifacts and wall paintings [17,18], diagnostic imaging, orthopedic medicines, and other biomedical applications [19–21].

Hitherto, several BaO Nanoparticles' (BaO-NPs) preparation routes have been developed to produce nanomaterials with different

sizes and shapes such as sol-gel, chemical method, hydrothermal, thermal decomposition, sonochemical, microwave irradiation, and quick-precipitation, etc. [17,18,22,23–28]. Among these preparation methods, the co-precipitation route has gained a lot of popularity in industries due to the facile way of synthesis, low temperature, and energy, cost-effective and inexpensive approach for good yield and large scale production.

The structural and optical properties of semiconductor nanoparticles have increasingly become a topic of great concern. In general, the nanoparticles' physical properties significantly depend on their microstructure, such as crystal defects, grain boundaries, as well as surface morphology. Therefore, to get a well understanding of the size-dependent physical properties of BaO-NPs, it is essential to acquire knowledge of their microstructure [1,17,18,22,23–28].

This paper presents the facile synthesis and characterization of BaO-NPs prepared through a novel, cost-effective co-precipitation route. The prepared nanoparticles' structural and optical properties were then analyzed through various characterization techniques such as X-ray Diffraction (XRD), Scanning Electron Microscopy (SEM), Energy Dispersion X-ray Spectrum (EDS), Fourier Transforms Infrared (FTIR), UV-Vis, and PL. Finally, important results were presented and discussed.

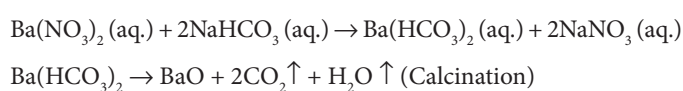
2. MATERIALS AND METHODS

2.1. Materials and Synthesis Process

Barium Nitrate [$\text{Ba}(\text{NO}_3)_2$] (Sigma-Aldrich, India, 98%) and Sodium Bicarbonate (NaHCO_3) (Merck, India, 98%) was used

*Corresponding author. Email: maansarivce@gmail.com

as a precursor and as a fuel respectively for the synthesis of BaO-NPs. BaO-NPs were prepared via a facile co-precipitation method. The schematic of the synthesis procedure is shown in Figure 1. In a typical synthesis, 0.5 M of $\text{Ba}(\text{NO}_3)_2$ was dissolved in 100 ml de-ionized water (H_2O), which was continuously stirred using a magnetic stirrer for approximately 30 min until the $\text{Ba}(\text{NO}_3)_2$ dissolved completely. The pre-prepared NaHCO_3 solution was added drop-wise into the $\text{Ba}(\text{NO}_3)_2$ solution, under vigorous stirring. After approximately, 2 h of continuous stirring the reaction white colored mixture forms completely. The produced mixture was kept for 12 h so that all constituent particles are get precipitated. The precipitated material was washed and centrifuged with distilled water and alcohol many times to eliminate the native impurities from the sample. Further, the precipitate was dried and calcined at 400–500 °C for 4 h in the air to ensure that $\text{Ba}(\text{HCO}_3)_2$ was converted into BaO completely. The whole reactions involve can be given as below:



2.2. Characterization

Structural characterization phase and crystallinity of as-synthesized BaO-NPs was done by using the XRD technique (Rigaku-Miniflex, Japan, X-ray diffractometer) using Cu $K\alpha$ radiations ($\lambda = 1.5406 \text{ \AA}$) in the 2θ range 20–80°. The morphology of as-prepared NPs was observed by FEI (Field Electron and Ion Company) Field Emission (FE)-SEM. FTIR spectroscopy (PerkinElmer, USA) was used in the 400–4000 cm^{-1} range for the analysis of chemical compositions of the prepared nanoparticles. UV-Vis (PerkinElmer) was used to obtain absorbance spectra of the NPs in the range from 200 to 800 nm at room temperature. PL spectra were recorded by using the Varian Carry Eclipse Fluorescence spectrophotometer (Agilent, California, USA).

3. RESULTS AND DISCUSSION

3.1. Structural and Morphological Properties

3.1.1. X-ray diffraction

Phase and crystallinity of as-synthesized BaO-NPs were done by using the XRD technique with Cu $K\alpha$ radiations ($\lambda = 1.5406 \text{ \AA}$)

in the 2θ range 20–60°. XRD spectra of synthesized BaO-NPs is shown in Figure 2. Many well-defined peaks correspond to various planes of BaO as (200), (201), (211), (102), (310) and (212), so on were seen in the observed XRD pattern which is all related and well-matched with the tetragonal phase of BaO-NPs and are in good agreement with the “JCPDS” card No. 26-0178. The observed results are also confirmed with the reported literature [23,26,28]. Sharp and intense peaks indicate the synthesized nanoparticles are highly crystalline in nature. The average crystallite size (D) of the sample is calculated using Debye-Scherrer's formula [29] which can be given as:

$$D = \frac{K\lambda}{\beta \cos \theta} \quad (1) [29]$$

where K is the shape factor (0.90), λ is the wavelength of Cu $K\alpha$ radiation ($\lambda = 1.5406 \text{ \AA}$), β is the full-width at half maximum, and θ is the diffraction angle. The average grain size of BaO-NPs is found to be ~16 nm.

3.1.2. Scanning electron microscopy

The morphology of the synthesized BaO-NPs was assessed by FE-SEM and presented in Figure 3a and 3b. Figure 3a shows a low-resolution (1500) image of prepared BaO-NPs which exhibits

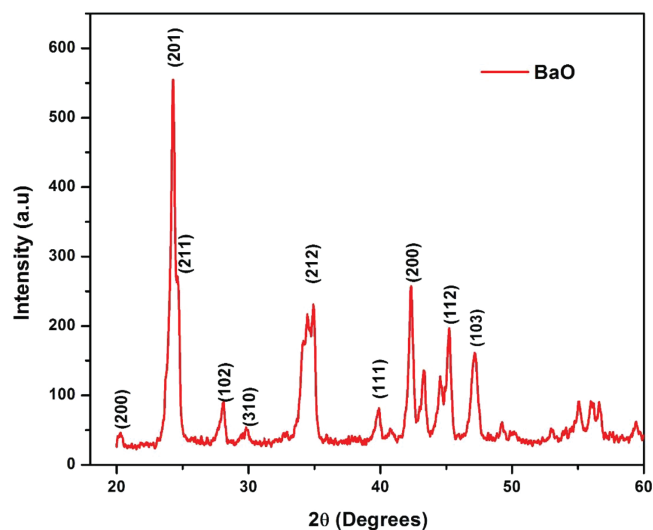


Figure 2 XRD pattern of as-synthesized BaO nanoparticles.

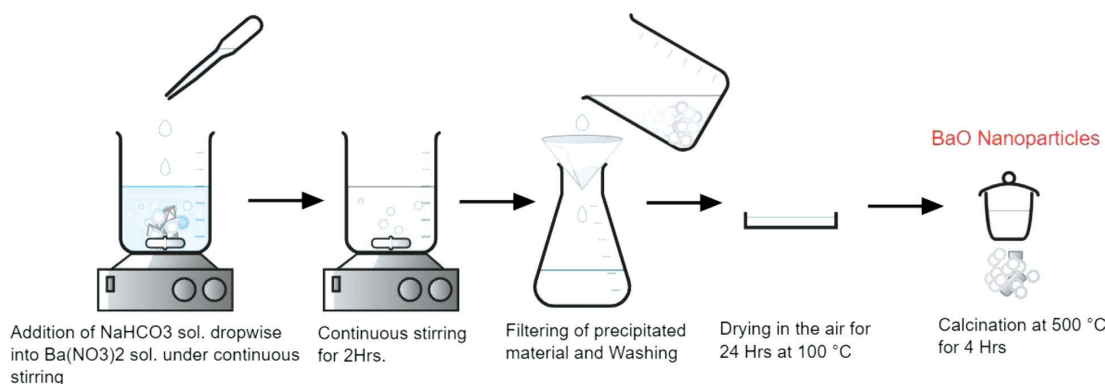


Figure 1 | Schematic of synthesis procedure of BaO nanoparticles.

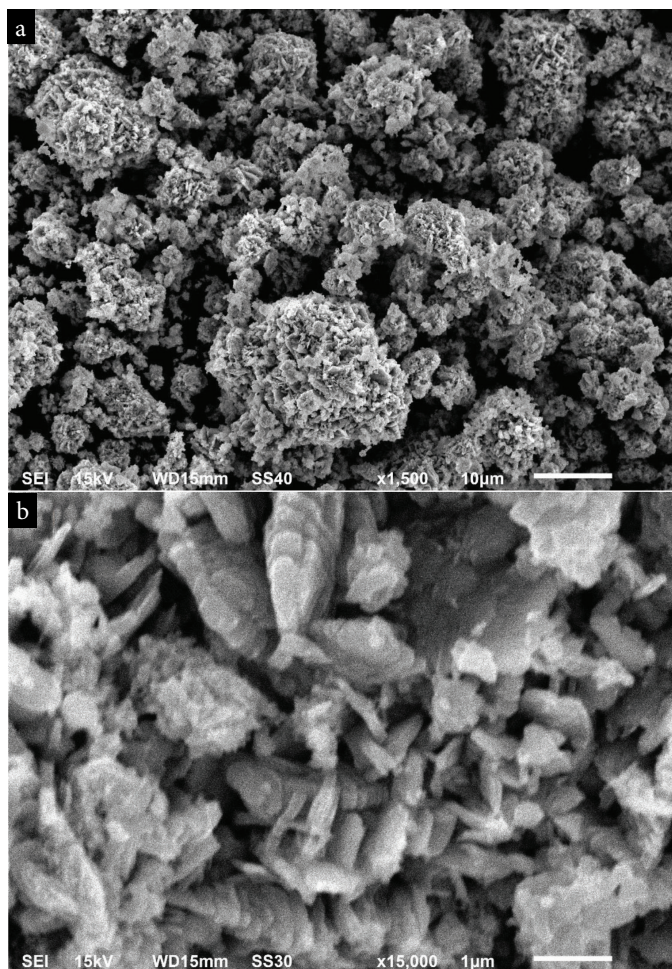


Figure 3 SEM images of BaO nanoparticles (a) at low magnification (b) at high magnification.

a flower-shaped clusters morphology. High-resolution SEM image is presented in [Figure 3b](#) shows the synthesized nanomaterials are grown highly crystalline. It can also be seen from the SEM images that some NPs are in nanorods and nanosheets like structures and are joined by accumulation on one above another. The elemental compositional analysis of synthesized NPs was assessed by EDS integrated to SEM. EDS spectra confirmed the chemical purity of synthesized BaO-NPs.

3.1.3. Fourier transform infrared

The chemical composition analysis of prepared BaO-NPs, was done with FTIR in the wavenumber range 4000–400/cm, and obtained results are presented in [Figure 4a](#) and [4b](#). The FTIR spectrum represents a strong absorption band at $\sim 692\text{ cm}^{-1}$ which corresponds to the Ba–O bond formation. A weak absorption band at $\sim 615\text{ cm}^{-1}$ also seen due to Ba–O stretching vibration. Two absorption bands observed at ~ 1754 and $\sim 3456\text{ cm}^{-1}$ in the FTIR spectra are associated with the O–H stretching and bending vibrations' modes, respectively. The peak at $\sim 1455\text{ cm}^{-1}$ is may be due to the barium carbonate formation which is result of absorption of atmospheric CO_2 by BaO-NPs. The peak seen at $\sim 1059\text{ cm}^{-1}$ is connected with O–O stretching modes of vibration [30].

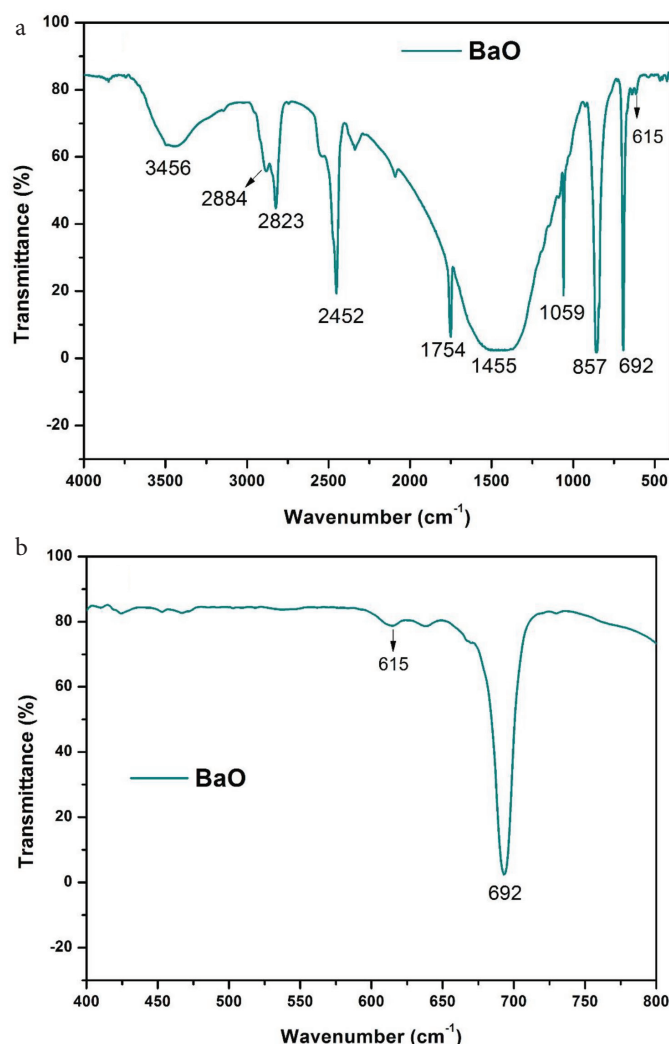


Figure 4 (a) FTIR spectrum of BaO nanoparticles and (b) enlarged view of spectra between region 400 and 800 cm^{-1} .

Two peaks at ~ 857 and $\sim 2452\text{ cm}^{-1}$ are associated with the asymmetric vibration modes of NO_3^- ions and $-\text{CO}_2$ bond vibration, respectively [28,31,32].

The results found are consistent with the previous literature [23,31,32]. No other absorption band associated to any other chemical group has been found in the FTIR spectra that indicate high purity of synthesized BaO-NPs sample.

3.2. Optical Properties

3.2.1. UV-Vis spectroscopy

The optical properties of synthesized BaO-NPs were examined by UV-Vis spectroscopy and the absorbance spectrum taken at room temperature is shown in [Figure 5](#). The measurement procedure followed was given in the literature [31,32].

The highest light absorption was noted at 310 nm, which is known as the characteristic edge or peak of BaO as reported in many literatures [1,23,28]. There is no other absorption peak was detected in

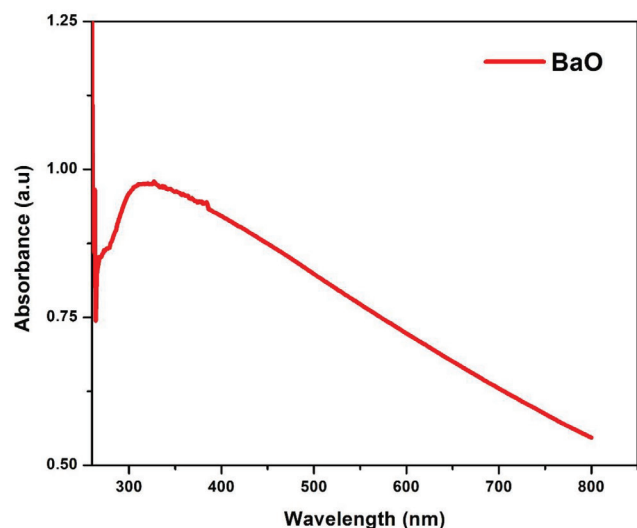


Figure 5 | Optical absorbance spectra of as-synthesized BaO nanoparticles.

the spectra that corroborates the possession of strong optical properties of the synthesized BaO-NPs.

The optical energy bandgap (E_g) of the prepared BaO-NPs was calculated by Tauc's relation [33,34], which provides the relation between the incident energy of the photon and the absorption coefficient of the semiconductor materials. The Tauc's equation can be given as:

$$(\alpha h\nu) = A (h\nu - E_g)^n \quad (2)$$

where A is a constant α is the optical absorption coefficient, $h\nu$ is the energy of the photon (where h is plank constant and ν is optical frequency), E_g is the optical band gap energy and n is an exponent its mathematical value relies heavily on the nature of the electronic transition causing the light absorption generally, n is taken equals 2 and 1/2 and for indirect and direct band gap, respectively.

Figure 6 shows the Tauc's plot for BaO NPs. The calculated optical bandgap energy (E_g) of as-prepared BaO NPs was 4.65 eV. The measured E_g is found very close to the bulk phase BaO and consistent with the previously reported literature [1,23,28]. The bandgap energy of nanophase BaO i.e. 4.65 eV is found higher than that of the bulk phase BaO i.e. 4.4 eV [10]. This enhancement in optical bandgap energy is because of the primarily known quantum size effect of nanophase materials. This theory (quantum size effect) applies only when the particle size is comparable to and in the range of de Broglie wavelength of a charge carrier (i.e. in the nanometer range).

3.2.2. Photoluminescence spectroscopy

Photoluminescence (PL) is the process of spontaneous light emission from the sample material when optically excited. The excitation energy and intensity can be chosen to probe different excitation types, determination of bandgap energy, identification of specific defects for radiative transitions, and impurity levels in the nanomaterial sample. Photoluminescence spectroscopy is a non-destructive analysis technique [6,35–37].

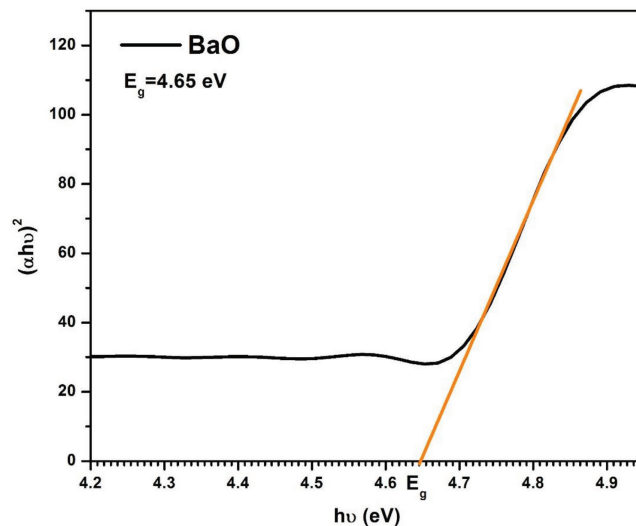


Figure 6 | Tauc-plot for energy bandgap calculation of as-synthesized BaO nanoparticles.

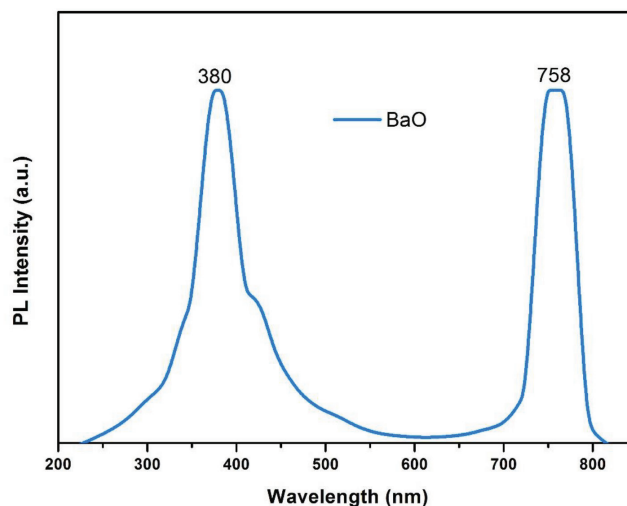


Figure 7 | Photoluminescence spectrum of BaO nanoparticles.

The photoluminescence spectrum of BaO-NPs was collected at the excitation wavelength of 230 nm and shown in Figure 7. The spectrum shows two major emission bands (Blue-violet and red). A total three number of peaks are detected which are as follows: a sharp emission peak at 380 nm, a broad peak at 410–574 nm may be because of the defects in the crystal of BaO, and a peak at 758 nm is may be due to an e–h pair recombination. Optical measurements result of UV–Vis and PL analysis show that the as-synthesized BaO-NPs can be expected as highly useful for optoelectronics and photonic systems and devices.

4. CONCLUSION

Highly crystalline BaO-NPs were successfully synthesized by the facile co-precipitation method and analyzed in detail through various materials analysis techniques. The results of the structural and chemical compositional analysis reveal a pure and highly-crystalline

tetragonal phase of BaO-NPs. The average grain size of BaO-NPs is found to be ~16 nm. The FE-SEM morphological analysis of the sample confirmed that the nanoparticles were grown highly crystalline. Also, some NPs are in nanorods and nanosheets like structures and are joined by accumulation on one above another. UV-Vis spectroscopy confirmed a significant optical properties of the sample and the calculated optical bandgap energy (E_g) of BaO-NPs was 4.65 eV which was found very close to the bulk phase BaO. A strong PL emission spectrum in the visible range making the as-synthesized BaO-NPs can be considered to be highly useful in optoelectronics and photonic systems and devices. The followed synthesis method can also be used in the preparation of other transition metal oxide nanomaterials.

CONFLICTS OF INTEREST

The authors declare they have no conflicts of interest.

AUTHORS' CONTRIBUTION

NJ contributed in conceptualization and in all graphs preparation. MAA carried out the experiment and wrote the original draft.

ACKNOWLEDGMENT

Authors are thankful to the Institute of ceramic and polymer engineering, University of Miskolc, Hungary for laboratories and valuable technical support.

REFERENCES

- [1] Renukadevi R, Sundaram R, Kasinathan K. Barium oxide nanoparticles with robust catalytic, photocatalytic and humidity sensing properties. *J Nanostruct* 2020;10:167–76.
- [2] Maity D, Agrawal DC. Synthesis of iron oxide nanoparticles under oxidizing environment and their stabilization in aqueous and non-aqueous media. *J Magn Magn Mater* 2007;308:46–55.
- [3] Guardia P, Pérez N, Labarta A, Batlle X. Controlled synthesis of iron oxide nanoparticles over a wide size range. *Langmuir* 2010;26:5843–7.
- [4] Wang L, Muhammed M. Synthesis of zinc oxide nanoparticles with controlled morphology. *J Mater Chem* 1999;9:2871–8.
- [5] El-Hofy M, Salama A. Synthesis and characterization of Ba defective ZnO nano-particle. In: Fisher DJ, editor. *Defect and diffusion forum*, Vols. 280–281. Switzerland: Trans Tech Publications Ltd; 2008, pp. 1–8.
- [6] Mohamed Basith N, Judith Vijaya J, John Kennedy L, Bououdina M. Structural, morphological, optical, and magnetic properties of Ni-doped CuO nanostructures prepared by a rapid microwave combustion method. *Mater Sci Semiconduct Process* 2014;17:110–18.
- [7] Sharma A, Sreenivas K, Gupta V, Tomar M. Room temperature detection of trace level NO₂ gas using SnO₂ nanoclusters. In: 2011 IEEE Sensors Applications Symposium. San Antonio, TX, USA: IEEE; 2011, pp. 145–8.
- [8] Chen YJ, Zhu CL, Wang LJ, Wang TH. One-pot synthesis of crystalline SnO₂ nanoparticles and their low-temperature ethanol sensing characteristics. *Sci China Ser G: Phys Mech Astron* 2009;52:1601–5.
- [9] Sankar R, Rizwana K, Shivashangari KS, Ravikumar V. Ultra-rapid photocatalytic activity of *Azadirachta indica* engineered colloidal titanium dioxide nanoparticles. *Appl Nanosci* 2015;5:731–6.
- [10] Cui Y, Chen J, Zhang Y, Zhang X, Lei W, Di Y, et al. Enhanced performance of thermal-assisted electron field emission based on barium oxide nanowire. *Appl Surf Sci* 2017;396:1108–12.
- [11] Umar A, Hahn YB. *Metal oxide nanostructures and their application*. Los Angeles, USA: American Scientific Publishers; 2010.
- [12] Renukadevi R, Sundaram R. Surfactant – free, facile synthesis of zinc tungstate nanoparticles for photocatalytic, antibacterial and humidity sensing applications. *Int J Tech Inn Mod Engg Sci* 2019;5:35–42.
- [13] Renukadevi R, Sundaram R. Synthesis, characterization, humidity sensing, antibacterial, photocatalytic and kinetic studies of novel HgWO₄-WO₃ nanocomposites. *Mater Today Proc* 2019;8: 153–61.
- [14] Zhang Y, Hou Y, Liu W, Zhang H, Zhang Y, Zhang Z, et al. A cost-effective relative humidity sensor based on side coupling induction technology. *Sensors (Basel)* 2017;17:944.
- [15] Choudhary VR, Jha R, Jana P. Epoxidation of styrene by TBHP to styrene oxide using barium oxide as a highly active/selective and reusable solid catalyst. *Green Chem* 2006;8:689–90.
- [16] Yang L, Choi YM, Qin W, Chen H, Blinn K, Liu M, et al. Promotion of water-mediated carbon removal by nanostructured barium oxide/nickel interfaces in solid oxide fuel cells. *Nat Commun* 2011;2:357.
- [17] Cordoncillo E, Machado TR, Ferrazza L, Juanes D. Synthesis and characterization of nanostructured BaO solutions: application in conservation of wall paintings. In: Ioannides M, Fritsch D, Leissner J, Davies R, Remondino F, Caffo R, editors. *Progress in Cultural Heritage Preservation. Euro-Mediterranean Conference*. Berlin, Heidelberg: Springer; 2012, pp. 801–8.
- [18] Saoud KM, Ibala I, El Ladki D, Ezzeldeen O, Saeed S. Microwave assisted preparation of calcium hydroxide and barium hydroxide nanoparticles and their application for conservation of cultural heritage. In: Ioannides M, Magnenat-Thalmann N, Fink E, Žarnić R, Yen AY, Quak E, editors. *Digital Heritage. Progress in Cultural Heritage: Documentation, Preservation, and Protection. Euro-Mediterranean Conference*. Cham: Springer; 2014, pp. 342–52.
- [19] Alarif S, Ali D, Al-Bishri W. In vitro apoptotic and DNA damaging potential of nanobarium oxide. *Int J Nanomedicine* 2016;11:249–57.
- [20] Gillani R, Ercan B, Qiao A, Webster TJ. Nanofunctionalized zirconia and barium sulfate particles as bone cement additives. *Int J Nanomedicine* 2010;5:1–11.
- [21] Hiraoka M, Ikeda K, Sano T. The mechanism of barium-induced automaticity in ventricular muscle fibers. *Adv Myocardiol* 1980;1:255–66.
- [22] Zeenath Bazeera A, Irfana Amrin M. Synthesis and characterization of barium oxide nanoparticles. *IOSR J Appl Phys* 2017;3:76–80.
- [23] Ahmad N, Wahab R, Alam M. Facile growth of barium oxide nanorods: structural and optical properties. *J Nanosci Nanotechnol* 2014;14:5342–6.
- [24] Devamani RHP, Alagar M. Synthesis and characterization of barium hydroxide nanoparticles. *Asian Acad Res J Multidisciplinary* 2014;1:60–75.
- [25] Mousa AO, Nema NA, Hasan HH. Effect of annealing on barium oxide (BaO) thin films prepared by chemical spray pyrolysis (CSP) technique. *J Chem Pharm Res* 2016;8:832–40.

- [26] Suresh G, Nirmala PN. Synthesis of barium oxide nanorod by chemical bath deposition. *Turk J Phys* 2012;36:392–7.
- [27] Prabhavathi SP, Punitha J, Rajam PS, Ranjith R, Suresh G, Mala N, et al. Simple methods of synthesis of copper oxide, zinc oxide, lead oxide and barium oxide nanoparticles. *J Chem Pharm Res* 2014;6:1472–8.
- [28] Sundharam E, Jeevaraj AKS, Chinnusamy C. Effect of ultrasonication on the synthesis of barium oxide nanoparticles. *J Bionanosci* 2017;11:310–14.
- [29] Dubal DP, Gund GS, Lokhande CD, Holze R. CuO cauliflower for supercapacitor application: novel potentiodynamic deposition. *Mater Res Bull* 2013;48:923–8.
- [30] Abramowitz S, Acquista N. The infrared spectrum of matrix isolated BaO₂. *J Res Natl Bur Stand A* 1971;75:23–5.
- [31] Chauhan MS, Kumar R, Umar A, Chauhan S, Kumar G, Faisal M, et al. Utilization of ZnO nanocones for the photocatalytic degradation of acridine orange. *J Nanosci Nanotechnol* 2011;11:4061–6.
- [32] Wahab R, Kim YS, Lee DS, Seo JM, Shin HS. Controlled synthesis of zinc oxide nanoneedles and their transformation to microflowers. *Sci Adv Mater* 2010;2:35–42.
- [33] Xiang Q, Yu J, Wang W, Jaroniec M. Nitrogen self-doped nanosized TiO₂ sheets with exposed {001} facets for enhanced visible-light photocatalytic activity. *Chem Commun (Camb)* 2011;47:6906–8.
- [34] Zhao W, Song X, Yin Z, Fan C, Chen G, Sun S. Self-assembly of ZnO nanosheets into nanoflowers at room temperature. *Mater Res Bull* 2008;43:3171–6.
- [35] Zhang YC, Tang JY, Wang GL, Zhang M, Hu XY. Facile synthesis of submicron Cu₂O and CuO crystallites from a solid metallorganic molecular precursor. *J Cryst Growth* 2006;294:278–82.
- [36] Yu T, Zhao X, Shen ZX, Wu YH, Su WH. Investigation of individual CuO nanorods by polarized micro-Raman scattering. *J Cryst Growth* 2004;268:590–5.
- [37] Al-Amri S, Shah Nawaz Ansari M, Rafique S, Aldhahri M, Rahimuddin S, Azam A, et al. Ni doped CuO nanoparticles: structural and optical characterizations. *Curr Nanosci* 2015;11:191–7.